SHAPE RECONSTRUCTION FROM VOLUMETRIC IMAGES

A Thesis Presented to The Faculty of the Graduate School

University of Missouri-Columbia

In Partial Fulfillment

Of the requirements for the Degree

Master of Science

---

by

Gregory Heckenberg

Dr. Ye Duan, Thesis Supervisor

August 2008

The undersigned, appointed by the Dean of the Graduate School, have examined the thesis entitled:

SHAPE RECONSTRUCTION FROM
VOLUMETRIC IMAGES

presented by Greg Heckenberg

a candidate for the degree of Master of Science and hereby certify that in their opinion it is worthy of acceptance.

Dr. Ye Duan

Dr. Jeffrey Uhlmann

Dr. Zhihai He

Acknowledgements

My thanks to my advisor, Dr. Ye Duan, for encouraging me to apply myself to many practical and interesting research problems. I have been well prepared to continue my education beyond graduate studies and become successful in further research areas and environments. His support and insights are deeply appreciated. Also, thank you to Yongjian Xi who provided much valuable feedback and collaboration during my time as a graduate student at the University of Missouri.

Contents

List of Figures

SHAPE RECONSTRUCTION FROM VOLUMETRIC IMAGES

Gregory Heckenberg

Dr. Ye Duan, Thesis Advisor

ABSTRACT

This thesis presents the research algorithms and techniques applied to three volumetric image problems(1) high quality mesh reconstruction from distance field volumetric data, (2) distance field surface approximation from gray scale images applied to 2-D and 3-D images, and (3) the extention of (2) to diffusion tensor magnetic resonance imaging (DT-MRI).

A proposed method for the extraction of high quality meshes from volumetric distance field data is given. The proposed method uses local gradient and curvature information to incrementally cover the objects surface by growing tangentially to the volume gradient.

An algorithm for structure inference of MRI brain data from 2-D and 3-D grayscale images is presented. Given a seed point initialization in a 2-D grayscale image, a PDE is proposed to evolve an explicit model based on the interior statistics of the previously identified region.

The algorithm is adapted to volumetric diffusion tensor MRI to extract the thalamus and thalamus nuclei structure. A modification of the mean shift algorithm is used to accomplish the segmentation of these more subtle structures.

1 Shape reconstruction from binary image data

1.1 Introduction

Surface extraction is an important operation for visualization and manipulation of volumetric data sets. Existing methods can be categorized into two groups: volumetric based cell decomposition approaches and surface-based region growing methods. The most popular volumetric-based approach is the Marching Cubes algorithm proposed by Lorenson and Cline[7].

In this section, a surface-based region growing procedure to extract a high quality mesh from an iso-surface is described. The algorithm is based on the idea of growing a mesh tangentially across a manifold defined by the underlying implicitly surface or volumetric representation. The algorithm can adapt to local surface curvature to better preserve sharp features as well as improve visual quality.

1.2 Algorithm

The algorithm consists of the following four main steps: (1) Seed initialization. (2) Create new contour points. (3) Create new boundary contour. (4) Local adaptive contour evolution.

1.3 Preprocessing

It may be desirable to "Smooth" purely binary data using a smoothing operation. This will allow for estimation of local gradients that better represent the surface structure. We use a multivariate Gaussian smoothing kernel to smooth binary data.

1.3.1 Seed initialization

The model is initialized by using a seed triangle on the surface to be extracted. The initial triangle is generated using the following algorithm. (1) Choose a starting point on the surface. This point can be chosen by the user or initialized

by choosing a boundary voxel defined by the volumetric data. At this point, a normal vector is defined by the volume data. (2) Find the first triangle edge by first finding a tangential vector using the cross product of the surface normal and a random vector. A point is chosen in this tangential direction and projected onto the surface. The distance from the initial point is determined by regulatory conditions (curvature, user maximum edge length, etc). (3) Complete the triangle by choosing a point in the tangential direction from the mid point of the edge found in step 2 subject to the same regulatory conditions. The three edges of this initial triangle define the surface's boundary contour.

1.3.2 Create new contour points

New points are created along the surface tangential direction from each boundary contour segment. Each point is then projected onto the iso-surface defined by the underlying volume data.

1.3.3 Create new boundary contour

Each edge then chooses the newly created contour point that had generated its edge. If the smallest sphere enclosing this candidate triangle does not contain any other contour points or points from the boundary contour, the triangle is created. Otherwise, search for the contour point that will satisfy this criteria using an iterative procedure of choosing one of the points enclosed in the candidate triangle's minimal enclosing sphere. This step may be repeated until a point that satisfies the condition is found. Edge flipping may also be necessary to ensure the sphere criteria holds for all previously created manifold triangles. Using the smallest enclosing sphere criteria ensures the extracted manifold is a Delaunay triangulation of the points on the manifold and encourages high quality mesh structure.

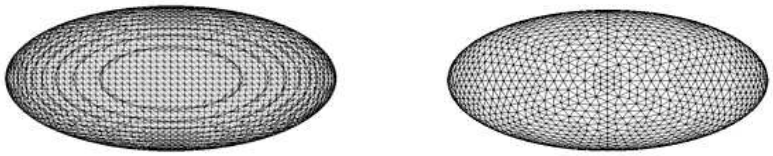

(a) Mesh generated using Marching Cubes algorithm

(b) Mesh generated using surface flow algorithm

Figure 1: Ellipsoid mesh rendered using described algorithm and Marching Cubes

1.3.4 Local adaptive contour evolution

The curvature regulatory conditions mentioned previously are implemented using an error-driven approach that checks the fitting error of each generated triangle. When the fitting error exceeds the threshold, the boundary contour is frozen until there are no further active countour edges. The step size is then reduced, and all previously frozen countour boundaries are reactivated. This adaptive step is repeated as necessary. The fitting error can be defined in a number of ways including surface distance to the iso-surface, maximum/Gaussian curvature, etc. The criteria used in our results is defined by the deviation of surface normals at each of the vertices of the triangle.

1.4 Experimental results

Figure 1 shows a comparison of the mesh extracted from volumetric ellipse data using the Marching Cubes algorithm and the described surface flow algorithm. These figures and the algorithm were presented in [9].

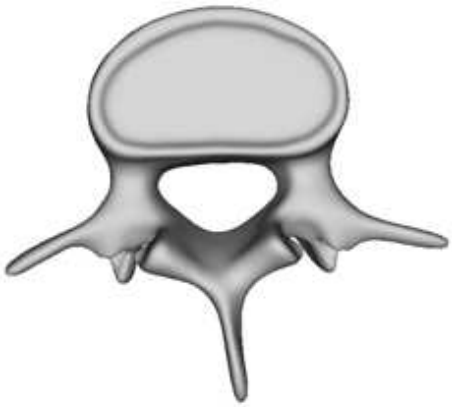

(a) Solid shaded view of extracted mesh

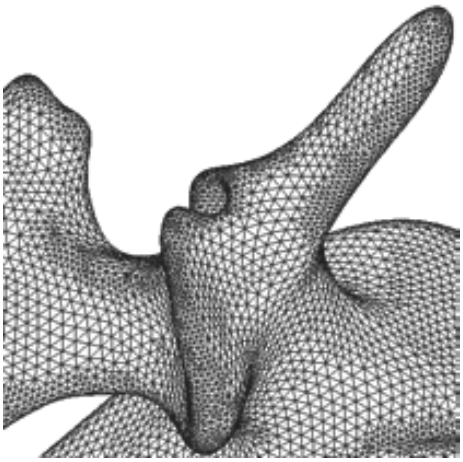

(b) Detailed view of mesh

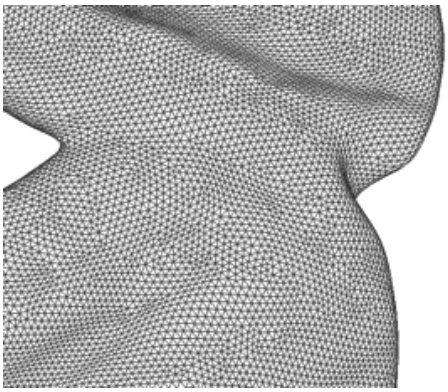

(c) Zoomed view of mesh

Figure 2: Volumetric vertebrae data

2 Shape reconstruction from gray scale volumetric data

2.1 Introduction

Extracting structural information from volumetric data is an extremely useful operation for many of today's data sets. Medical imaging modalities including CT and MRI have provided large data sets that can be analyzed for visualization or comparative procedures. These data sets do not provide binary data, but rather an estimate of signal over the volume. Inferring the structure of the underlying object is necessary when determining the binary segmentation.

2.2 Model description

2.2.1 Geometric surface flow

This new segmentation framework is based on the concept of geometric surface flow. The general formulation of the geometric surface flow is the following system nonlinear PDEs:

$$\frac{ds(p)}{dt} = F(t, k, k', f, ...) \cdot n(p, t), s(p, 0) = s_0(p) \tag{1}$$

where F is the speed function, t is the time variable, k and k' are the surface curvature and its derivative at the point s, $s_0(p)$ is the initial surface, n is the surface normal vector.

The function F used in 1 is described below.

2.2.2 Thalamus segmentation

When applying the above geometric surface flow for thalamus segmentation, the speed function F in 1 is explicitly formulated as a linear combination of the following two terms:

$$F = \alpha_1 F_{reg} + F_{data} \tag{2}$$

here F_{reg} is the regularity term to maintain the smoothness of the model. F_{reg} is usually a function of the curvature (e.g., mean curvature, Gaussian curvature). In this work, F_{reg} is defined as the difference between the mean curvature, H_{curr} at the local surface and the average mean curvature, H_{avg} calculated from the whole curve:

$$F_{reg} = H_{curr} - H_{avg} \tag{3}$$

F_{data} is defined by the current state of the model as well as the local data. Often F_{data} will model edge information in the image, However, since the thalamus has low contrast, using boundary information alone is not reliable. To improve the performance, a term influenced by the model's interior region information is included in the model as suggested by Huang et al. [5]. In particular, we define F_{data} as a linear combination of the two terms:

$$F_{data} = \alpha_2 F_{edge} + \alpha_3 F_{region} \tag{4}$$

F_{edge} is a function of the image's edge information influencing the contour to move towards edges.

$$F_{edge} = -\Delta(G_\sigma \star I(s)) \tag{5}$$

where Δ is the Laplacian operator, I is the image intensity function, and $G_\sigma \star I$ is the smoothed intensity function by convolution with a Gaussian filter with variance σ. Variance σ can be assigned according to the image resolution of the MRI data set. In our experiment, σ is set as 1.0.

F_{region} influences the contour based on the current model's interior statistic estimates.

$$\begin{aligned} d &= min\{.5 + .5 * (P(s|M) - P_{avg,M})/P_{avg,M}, 1\} \\ F_{region} &= cos(2\pi d) \end{aligned} \tag{6}$$

$P(s|M)$ is the probability of observing $I(s)$, the intensity of surface point s, given the interior probability estimation of the current model, M (see equation 11, which will be explained in more detail in the following sections. $P_{avg,M}$ is the average probability for all voxels given the current model. The variable d is used for notational convenience, representing the linearly interpolated probability, capped at a maximum of 1. F_{region} is a cosine interpolation of the linearly transformed probability of a surface point being consistent with the current model's interior. F_{region} will expand the contour outwards in regions that are considered compatible with the current segmented volumes statistics and contract from voxels that are not similar to the current model's interior.

The full form of the speed function is obtained by substituting 3, 4, 5, and 6 into 2:

$$\begin{aligned} F &= \alpha_1(H_{curr} - H_{avg}) - \alpha_2\Delta(G_\sigma \star I(s)) \\ &\quad +\alpha_3 cos(2\pi min\{.5 + .5 * (P(s|M) - P_{avg,M})/P_{avg,M}, 1\}) \end{aligned} \tag{7}$$

Here, α_1, α_2, α_3, are the corresponding weighting coefficients. In the results that follow, these parameters take on the values 0.1, 0.1, 1, respectively.

2.2.3 Algorithm description

The following is an outline of the algorithm. Each of the steps will be described in the following paragraphs.

1) seed initialization

2) Interior statistics estimation

3) Model evolution

4) Iterate steps 2-4 until convergence

5) Binary image creation

Seed initialization To initialize the model, the user interactively selects a pixel/voxel inside the region of interest in the image data. A circular contour

centered at the pixel/voxel is then automatically created and serves as the initial model.

Interior statistics estimation Given the current model interior, a probability density function is estimated. We use a non-parametric density estimator, the Parzen window based nonparametric method [2] because it is differentiable and can represent complex multimodal intensity distributions. We choose the Gaussian kernel as the Parzen window function. Suppose the model M is placed on an image I, the volume of the image region included by the current model M is V, then the probability of a pixels (or in 3 dimensions, voxels) intensity value i being drawn from the distribution of the model interior can be derived as

$$P(i|M) = \frac{1}{|V|} \int_V \frac{1}{\sqrt{2\pi}\sigma} e^{-(i-I(x))^2/2\sigma^2} dx \tag{8}$$

where σ is a constant that specifies the width of the Gaussian kernel and is set as 1.0 in our experiment. Since 8 is a simple integral, it can be calculated very efficiently as an incremental update such that only newly added or removed pixels/voxels are used to update the integral value at each time step for each intensity value i. This update can be performed in time proportional to model's perimeter rather than its area (surface area, volume in 3 dimensions).

Model evolution Finally, the model will evolve according to 1 and 7. More specifically, the surface evolution process is numerically approximated using a simple iterative equation:

$$S(p, t + \Delta t) = S(p, t) + F(p, t)N(p, t)\Delta t \tag{9}$$

When advancing the model, a constraint on the size of the time step Δt is necessary. In particular, the model update during time step Δt must satisfy stability conditions. Specifically, the maximum change must be strictly restrained by the minimum detail in the system. This is accomplished by ensuring any

iterative change in the model does not exceed more than one voxel.

$$\Delta t \leq \frac{l}{max(S(p_i, t + \Delta t) - S(p_i, t))} \tag{10}$$

where l is the unit grid edge length of the image data. Before each deformation step, the velocity F is calculated at each explicitly represented surface point and used to determine the maximum velocity for the current evolution step. A proper time step can then be estimated using 10.

Test of convergence After each deformation cycle, the model will loop from step 2 to step 4 until an equilibrium state is achieved. Convergence can be checked using the maximum surface change or a fixed amount of time has passed. The deformation is halted and the geometry of the thalamus can be extracted from the MRI binary image.

Binary image creation Next, based on the interior probability density distribution of model M obtained in the previous step, the image intensity probability map $P(i|M)$ of every pixels (voxels) intensity is obtained. A small threshold (e.g., the mean $P(i|M)$ over the entire image domain) is applied to produce a binary image $B(i|M)$

$$B(i|M) = \begin{cases} 1, & P(i|M) > \sum_{j=1}^{n} P(j|m)/n \\ 0, & otherwise \end{cases} \tag{11}$$

2.3 Model description

At each step of the two dimensional model, the current boundary is explicitly represented by connected points on the front. Each of these points is propagated using 7, while maintaining the connections. Regularity in point spacing is maintained by adding points to edges with a length greater than the maximum edge length, or by removing points that are connected by edges shorter than the minimum edge length. Intersection is handled by checking for segment overlaps.

For the 3 dimensional model, maintaining connectivity as well as surface intersection is much more complex. For this case, an explicit point representation is used with surface resampling. This provides more flexible intersection handling, while avoiding complex mesh topology operations. The speed function is applied to each of the sampled surface points as they are propagated. The volume grid is updated with the distance to the nearest point, and the points are resampled. This update operation need only be carried out on those voxels containing the boundary contour, rather than the whole volume.

2.4 Experimental results

A result using this algorithm is shown in Figure 3 for segmenting a 2D image of the thalamus. The binary mask for at each intermediate model state is shown in Figure 4 for each model contour in Figure 3. Each of the two figures shows five intermediate model states from the seed (Figure 3(a)) through to the final segmentation (Figure 3(e)).

Figure 5 is a similar series of images showing the model evolution (5(a)-5(d)) on three dimensional data. Visualization of the brain is accomplished by displaying three orthogonal slices of the MRI data with the current model's boundary shown in green. Figure 5(e) shows the side profile of the segmented thalamus.

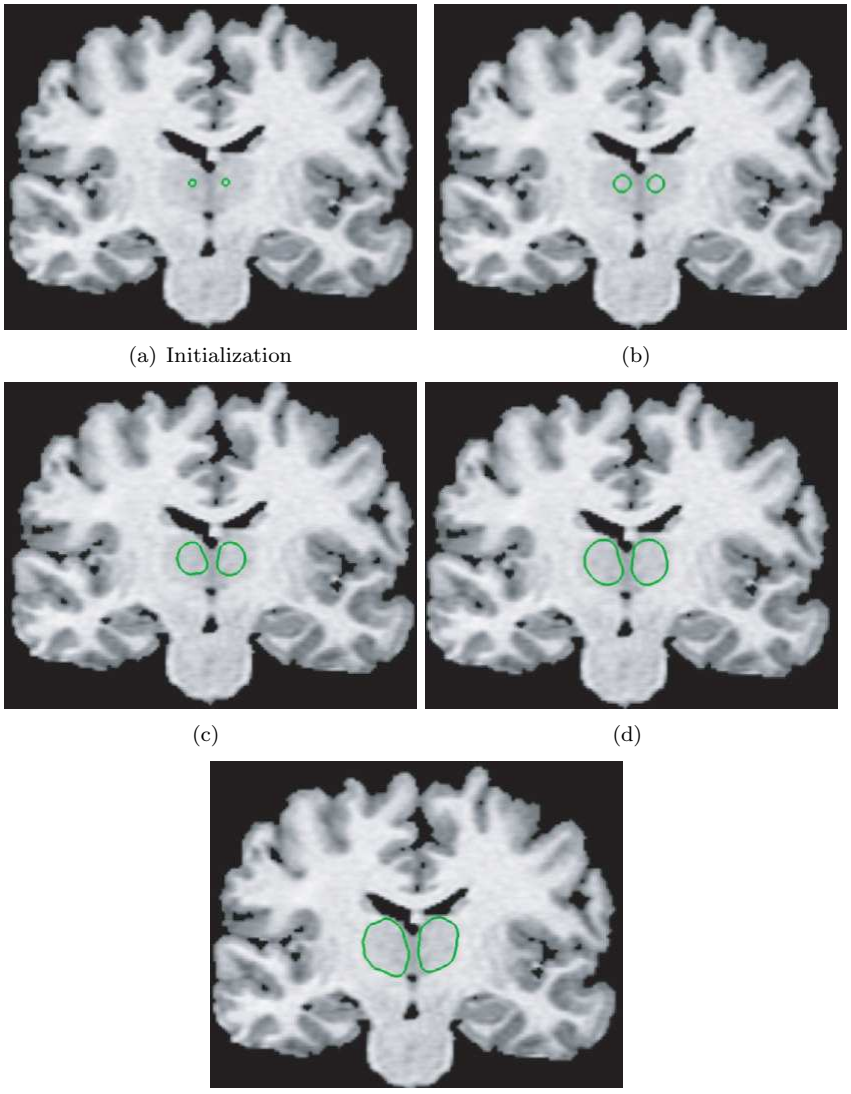

(a) Initialization (b)

(c) (d)

(e) Final segmentation

Figure 3: Progression from initialization to final segmentation of a 2d image

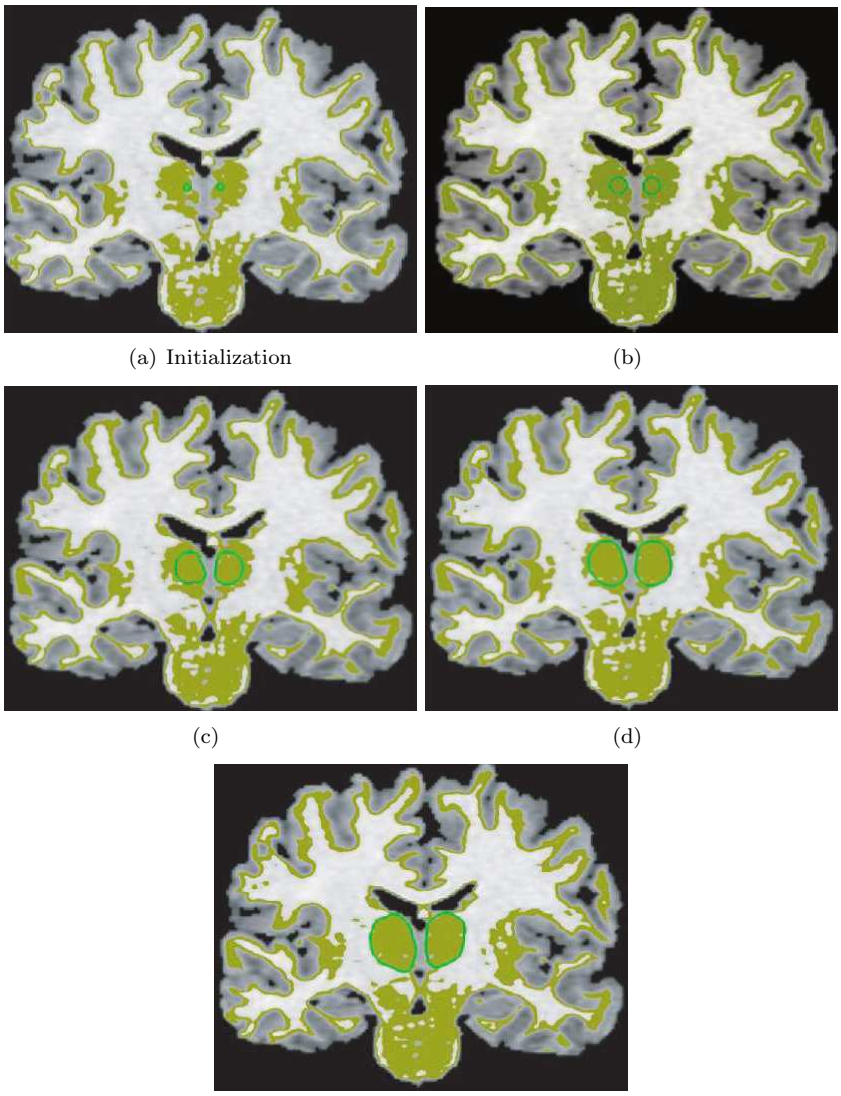

(a) Initialization (b)

(c) (d)

(e) Final segmentation

Figure 4: Binary mask at each model state

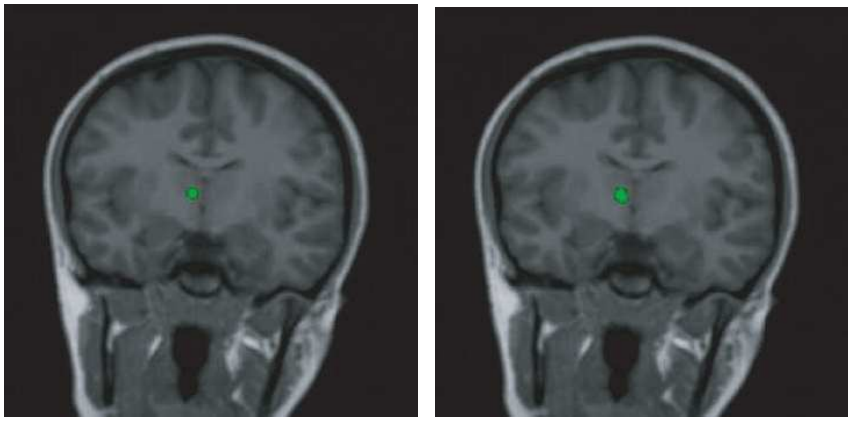

(a) Initialization (b)

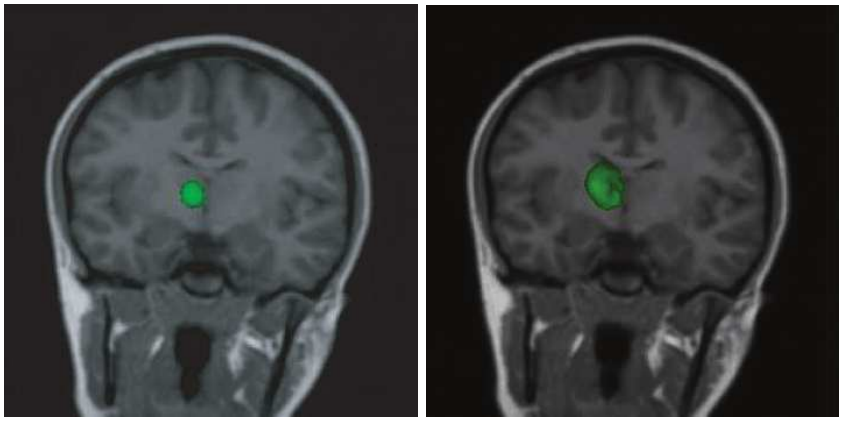

(c) (d) Final

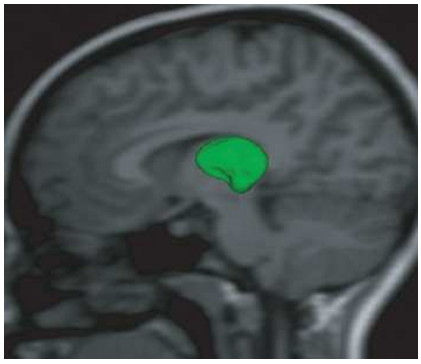

(e) Profile of final segmentation

Figure 5: Thalamus segmentation on a 3d data set progressing from initialization to final segmentation

3 Shape reconstruction from tensor volume data

3.1 Thalamus introduction

The thalamus is a very important brain structure considered part of the limbic system. It serves as the relay center for nerve impulses in the brain, mediating communications between sensory, motor, and associative brain regions. The thalamus receives information from many diverse areas of the brain then sends this information on the the cerebral cortex. The thalamus plays a major role in the regulation of consciousness, alertness, arousal, and attention.

The thalamus region consists of two lobe masses of gray matter located in the mid brain. Each lobe is about four centimeters in length. It is surrounded by cerebral spinal fluid (CSF) and fiber bundles in the white matter connecting the region to the outer cortex. Each thalamus itself is further divided into smaller nuclei structures which serve different purposes.

Variations in thalamus and white matter characteristics have been linked to a large number of diseases including, schizophrenia, Parkinson's disease, and multiple sclerosis. Studying the structure and properties of the thalamus may lead to important breakthroughs in these fields. Conventional imaging modalities, such as Computerized Tomography (CT) and Magnetic Resonance Imaging (MRI), do not provide the necessary image contrast or resolution to differentiate the individual thalamic nuclei.

Diffusion Tensor MRI, has been proposed to give more information about the nerve structures within the brain. DT-MRI represents the local average diffusion through brain matter as a tensor. In nerve fibers, this diffusion is highly anisotropic as cell membranes restrict the motion along the boundary. DT-MRI has already been used to study and visualize brain connectivity through white matter through the use of stream tracing[6]. Stream tracing uses the primary eigenvector to determine the most likely direction of nerve fiber continuation.

The fiber is traced from its beginning to its end, and the procedure is repeated for all areas of high anisotropy.

The intention of this work is to use the diffusion tensor information to gain more information about the structure of the thalamus. Gray matter composing the thalamus is distinguishable from white matter using traditional MRI[4], however, it does not give sufficient discrimination of smaller structures within the thalamus. This work uses local tensor similarity to guide the understanding of these regions using non-invasive MRI images. The potential applications may be for diagnosing disorders or planning surgery without the need for invasive surgery.

3.2 Background

This work incorporates the additional structure information available through Diffusion Tensor Magnetic Resonance Imaging modalities and incorporates the mean shift [3] segmentation framework. Brief overviews of these two topics is provided below.

Diffusion tensor imaging Diffusion Tensor Magnetic Resonance Imaging (DTMRI) is a recent MR imaging modality. In Diffusion Tensor MRI, a tensor describing local water diffusion is acquired for each voxel. This tensor characterizes the local tissue structure. A good review on DT-MRI can be found in [1] and [8].

At each voxel location, a symmetric 3x3 diffusion tensor, D, with six degrees of freedom is estimated. To estimate the tensor at each voxel, at least six measurements (taken from different non-collinear gradient directions) are taken in addition to the baseline image data S_0. These seven images are collected for each slice in the data set with different diffusion weightings and gradient directions.

Let S_0 represents the signal intensity in the absence of a diffusion-sensitizing field gradient and S_k the signal intensity in the presence of gradient gk =

(gkx, gky, gkz), $k = 1, ..., 6$. the equation for the loss in signal intensity due to diffusion is given by the Stejskal-Tanner formula:

$$ln(S_k) = ln(S_0) - \gamma^2\delta^2(\Delta - \delta/3)g^T Dg \tag{12}$$

where γ is the gyromagnetic ratio of hydrogen H (protons), δ is the duration of the diffusion sensitizing gradient pulses and Δ is the time between the centers of the two pulses. The tensor D can then be computed by solving this system of six equations (Eq. 12).

Mean shift clustering Mean shift is a powerful general purpose technique for clustering scattered data [3]. Instead of an *a priori* assumption of a fixed number of clusters, mean shift assigns each element to the cluster representing its mode.

Given an arbitrary set of n points $X = x_1, ..., x_n$ in the d-dimensional Euclidean space R_d. The multivariate kernel density estimate obtained with kernel $K(x)$ and window radius h, computed in the point x is defined as:

$$\hat{f}(x) = \frac{1}{nh^d}\sum_{i=1}^{n} K(\frac{x - x_i}{h}) \tag{13}$$

The smoothing bandwidth parameter h determines the density function smoothness. $K(x)$ is the radially symmetric kernel satisfying

$$K(x) = c_{k,d}k(\|x\|^2),$$

$$k(x) \geq 0,$$

$$\int_{R^d} K(x)dx = 1$$

Assume now that we are interested in subdividing scattered data into a set of clusters. To determine which mode of $\hat{f}$ a point belongs, a gradient ascent algorithm is employed. The gradient for iteration is found by differentiating 13.

$$\nabla \hat{f}(x) = \frac{2c}{nh^{d+2}} \sum_{i=1}^{n} g(\|\frac{x - x_i}{h}\|^2) m(x) \tag{14}$$

where $g(x) = k(x)$. $m(x)$ is the mean shift vector.

$$m(x) = \frac{\sum_{i=1}^{n} x_i g(\|\frac{x-x_i}{h}\|^2)}{\sum_{i=1}^{n} g(\|\frac{x-x_i}{h}\|^2)} - x \tag{15}$$

The mean shift vector represents the difference between the position, x, and the neighborhood mean, using the kernel g to define the local neighborhood weights. The general mean shift clustering procedure consists of the following two steps:

1) Initialize: $y_0 = x$

2) Iterate $y_{j+1} = y_j + m(y_j)$ until convergence. In the case when each point

x_i in the data set has two components of different nature, i.e. $x_i = (p_i, q_i)$: $p_i P, q_i Q$, the mean shift algorithm can be extended with separable kernels:

$$\hat{f}(x) = \frac{1}{nh_1^{d_1} h_2^{d_2}} \sum_{i=1}^{n} K_1(\frac{p - p_i}{h_1}) K_2(\frac{q - q_i}{h_2}) \tag{16}$$

These two components are referred to as spatial and range components. In a 2d image, the spatial component may refer to the pixel coordinates, while the range component is defined by the color at each pixel.

3.3 Thalamus and thalamus nuclei segmentation

To adapt the meanshift algorithm for use on DT-MRI data, a separable kernel approach is used as defined in 16. The kernel function K_1 represents the normal

Since there are two different domains of similarity (tensor and spatial) in the DT-MRI image data, the extended mean shift algorithm with separable kernels as defined by Eq. 16 is used. The K_1 kernel is defined over in the tensor domain with parameter h_1,

In the tensor domain, choose k is chosen to be a normal kernel and distance metric, d based on the Frobenius norm between two matrices:

$$d(D_1, D_2) = \sqrt{Trace((D_1 - D_2)(D_1 - D_2)^T)} \tag{17}$$

D_1 ,D_2 are the tensor matrices at positions x_1, x_2, respectively.

K_2 is the kernel in the tensor domain with parameter h_2. In the spatial domain, the kernel function $K_2(x)$ is chosen to be the normal kernel with the Euclidian distance metric defined over 3-dimensional space. The spatial bandwidth parameter h_2 chosen determines the scale of features detected, so different values can be chosen based on the data set quality and size of features of interest.

3.4 Results

Figure 3.4 shows a 2D sliced view of the mean-shift based segmentation result at both the thalamus as well as the thalamus nuclei level. More specifically, Figure 6(a) is the segmentation result by using a 5 by 5 by 2 bandwidth, while Figure 6(b) is the segmentation result obtained by a 3 by 3 by 1 bandwidth. From Figure 6(a), the anterior and posterior regions of the thalamus are clearly segmented. With the choice of a smaller h_2, more detailed nuclei structures are found (Figure 6(b)), which can be compared to the histological atlas of the human thalamus sub nuclei structure 6(c).

Each of these segmentation results were generated from presegmented data of the total thalamus structure from the gray scale MRI data. This is possible since the thalamus is surrounded by relatively homogeneous structures such as fiber tracts and CSF. The initially segmented thalamus will then serve as the mask for the subsequent thalamus nuclei segmentation, which will be conducted automatically with a smaller bandwidth parameter. A 3D rendering of the thalamus nuclei segmentation result is shown in Figure 6.

In these results, the bandwidth parameter h_1 was set as 1. To achieve consistent thalamus segmentation results the bandwidth parameter h_2 used in

x, y, z dimensions were 5, 5, 2, respectively. For thalamus nuclei segmentation, a smaller bandwidth such as 3, 3, 1 was used. The non-uniform scale of the parameter in the z dimension is due to the low resolution of the image data in the z dimension.

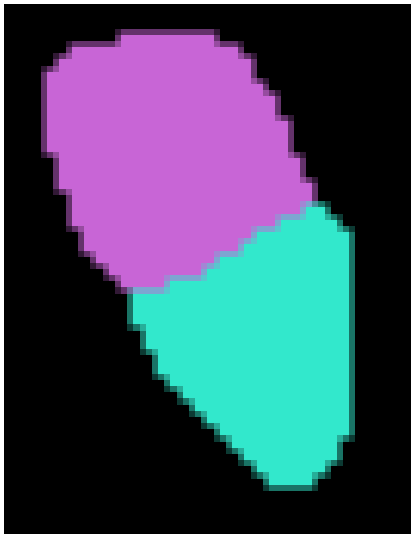

(a) Anterior and posterior thalamus segmentation

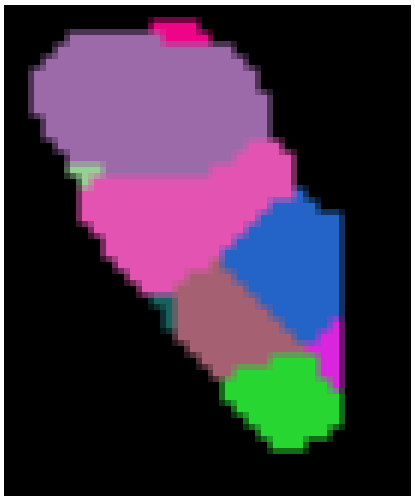

(b) Sub-nuclei thalamus segmentation

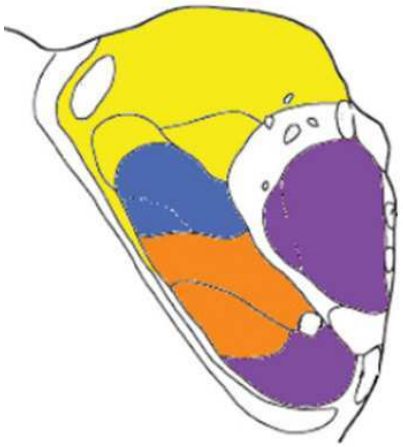

(c) The histological atlas of the human thalamus

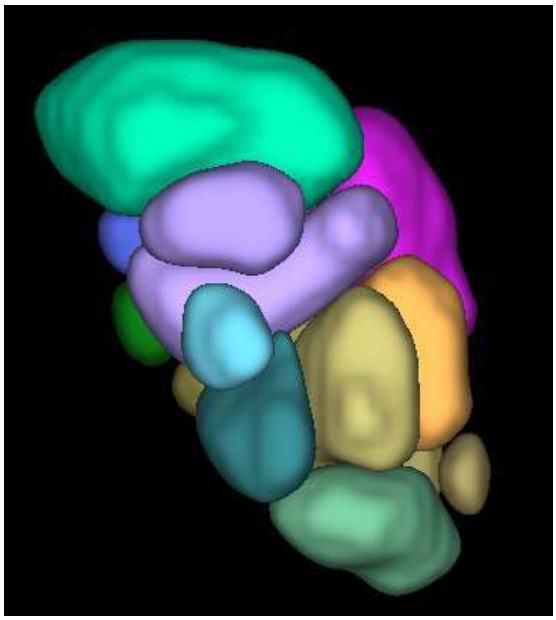

Figure 6: 3d volumetric rendering of nuclei structure

4 Conclusion and future work

In this work, an algorithm for extracting course features from grayscale volumetric images has been presented. The algorithm is efficient and relies only on a user specified seed point to identify the region of interest. The specific application to MRI data is presented in the result examples. In addition, to this segmentation of large structural features from grayscale data, an algorithm for further refinement of thalamus nuclei is presented to take advantage of the additional information available through Diffusion Tensor Magnetic Resonance Imaging modalities. Once structures have been identified, high quality meshes can be constructed using the presented geometric surface flow algorithm.

In the future, this work may be extended to include more comprehensive structural segmentation from DT-MRI such as nerve fiber bundles. The connectivity of each nuclei to the cortex may be extracted to study variations in connectivity in patients. In addition, the incorporation of additional imaging modalities (e.g. functional MRI) may allow for improved interpretation and analysis of observed brain activity patterns.

While the thalamus is a relatively easy ROI to determine from plain MRI images (high contrast compared to surrounding regions with homogeneous intensity), in the future, the segmentation framework may be extended to incorporate texture information within the structure to make it more applicable to general segmentation applications. As an example, tumors often have heterogeneous tissue composition which are more difficult to segment using the current distribution estimation processes.

In addition, simultaneously segmenting the surrounding regions as well as the thalamus ROI may provide better results by adding a more competitive criteria at the boundaries. This may improve the detection of edges within textured regions when compared to using the Laplace of Gaussian edge detection methodology.

References

[1] P.J. Basser, S. Pajevic, C. Pierpaoli, J. Duda, and A. Aldroubi. In vivo fiber tractography using dt-mri data. *Magn Reson Med*.

[2] C.M.Bishop. *Neural Networks for Pattren Recognition*. Oxford University Press, Oxford, UK, 1995.

[3] D. Comaniciu and P. Meer. Mean shift: A robust approach toward feature space analysis. *PAMI*, 24(1):603–619, May 2002.

[4] Greg Heckenberg, Yongjian Xi, Ye Duan, and Jing Hua. Brain structure segmentation from mri by geometric surface flow. *International Journal of Biomedical Imaging*, 2006.

[5] X. Huang, D. Metaxas, and T. Chen. Metamorphs: Deformable shape and texture models. *Journal Proceedings of IEEE Conference on Computer Vision and Pattern Recognition*, pages 496–503, 2004.

[6] L. Jonasson, X. Bresson, P. Hagmann, O. Cuisenaire, R. Meuli, and J. Thiran. White matter fiber tract segmentation in dt-mri using geometric flows. *Medical Image Analysis*, 9(3):223–236, 2005.

[7] W. E. Lorensen and H. E. Cline. Marching cubes: A high resolution 3d surface construction algorithm. *Proceedings of SIGGRAPH*, 21:163.

[8] C.-F. Westin, S.E. Maier, H. Mamata, A. Nabavi, F.A. Jolesz, and R. Kikinis. Processing and visualization for diffusion tensor mri. *Medical Image Analysis*, 6:93–108, 2002.

[9] Yongjian Xi, Greg Heckenberg, Ye Duan, and Jin Hua. Iso-surface extraction by front propagation. *Proceedings of Pacific Graphics 2005, Macao, China*, 2005.